

A MEASUREMENT OF THE Ni<sup>60</sup> DIRECTIONAL CORRELATION  
WITH A TUNNEL DIODE COINCIDENCE CIRCUIT

by

GARY EDWIN CLARK

B. A., Park College, 1961

---

A MASTER'S THESIS

submitted in partial fulfillment of the

requirements for the degree

MASTER OF SCIENCE

Department of Physics

KANSAS STATE UNIVERSITY  
Manhattan, Kansas

1966

Approved by:

*Louis D. Elwood*

---

Major Professor

LD  
266F  
T4  
1966  
C57  
C.2

TABLE OF CONTENTS

Document

I.	INTRODUCTION . . . . .	1
	1. Purpose of the Paper . . . . .	1
	2. Review of Literature . . . . .	2
II.	TUNNEL DIODE COINCIDENCE CIRCUIT . . . . .	3
	1. Properties of the Tunnel Diode . . . . .	3
	2. The Univibrator Circuit . . . . .	5
	3. Detection of Coincident Pulses . . . . .	9
	4. Zero Crossover . . . . .	10
	5. Noise and Feedthrough . . . . .	11
	6. Slewing . . . . .	12
	7. Effect of Temperature . . . . .	14
	8. Jitter . . . . .	14
	9. Nanosecond Systems, Inc., Equipment . . . . .	14
III.	THEORY OF DIRECTIONAL CORRELATION . . . . .	17
	1. The Directional Correlation Function . . . . .	17
	2. The Ni <sup>60</sup> Cascade . . . . .	20
	3. Analysis of Chance Rates . . . . .	21
	4. Experimental Considerations . . . . .	24
	5. Correction for Finite-Size Detectors . . . . .	27
IV.	MEASUREMENT OF THE Ni <sup>60</sup> DIRECTIONAL CORRELATION . . . . .	31
	1. Apparatus . . . . .	31
	2. Determination of Resolving Times . . . . .	32
	3. Determination of Chance Rates . . . . .	33
	4. Determination of Correction for Finite- Size Detectors . . . . .	34
	5. Reduction of Error at 135° . . . . .	35
	6. Analysis of Ni <sup>60</sup> Correlation Data . . . . .	36
V.	CONCLUSION . . . . .	41
VI.	ACKNOWLEDGMENTS . . . . .	42
VII.	PLATES . . . . .	43
VIII.	REFERENCES . . . . .	73

## I. INTRODUCTION

### 1. Purpose of the Paper

In nuclear spectrometry scintillation materials and photomultiplier tubes are frequently used which produce electrical pulses with two useful parameters, pulse height and time of occurrence. In this paper we are concerned with the second parameter and in particular a method of determining whether or not two pulses occur coincidentally within a few nanoseconds ( $10^{-9}$  seconds) or less. Tunnel diodes, which are sometimes called Esaki diodes, are a suitable choice for a coincidence circuit for several reasons: They have fast switching times, can be very much overdriven without harmful effects, consume little power, and require only a small signal. Furthermore they are insensitive to humidity variations, can operate over a wide temperature range, and withstand neutron irradiation.<sup>8</sup> The fact that they are two-terminal devices, and therefore not unidirectional, is a large disadvantage which can be somewhat overcome by careful circuit design.

A tunnel diode coincidence circuit similar to the one described by Whetstone<sup>48</sup> was constructed and its properties are discussed in the second part of the paper. One application of coincidence circuits is in the measurement of a directional correlation, the theory of which is treated in Part III. The experimental determination of the directional correlation function of the Ni<sup>60</sup> cascade using this circuit is given in Part IV. Sufficient evidence is presented to indicate that the circuit

can be used for this type of measurement. Before proceeding with the main part of this paper a short review of the literature is presented.

## 2. Review of Literature

Scintillation methods have been employed in nuclear physics since the beginning,<sup>31</sup> while coincidence techniques were used as early as 1929.<sup>15,38</sup> Although most present day fast coincidence circuits utilize solid state devices, early circuits built by Rossi and others had vacuum tubes only.<sup>4,12,16,20,28,41</sup> A few circuits are reported which combine tunnel diodes and vacuum tubes<sup>10</sup> or tunnel diodes and transistors.<sup>1,35,46</sup> Avalanche transistors have been employed but not extensively.<sup>2,13</sup> The complexity of coincidence circuits ranges from a simple circuit of crystal diodes<sup>3</sup> to extremely complex combinations of electronic devices.

There are many variations of the fairly simple and highly reliable circuit with which the paper is concerned.<sup>23,24,26,45,47,48</sup> The basic building block (see Plate II) of such a circuit is the tunnel diode univibrator, which can handle counting rates in excess of 100 Mc/s provided dead time is properly controlled.<sup>1,49</sup> Because tunnel diodes have extremely small switching times, this circuit is advantageous when a very small coincidence resolving time is desired.

A word must be said about gallium arsenide tunnel diodes, which were considered very unreliable a few years ago. Gallium

arsenide tunnel diodes, when not subjected to continuous voltage high above the forward point, and germanium tunnel diodes are now equally reliable and are available at reasonable prices. Their various properties will be discussed in the next section.

## II. TUNNEL DIODE COINCIDENCE CIRCUIT

### 1. Properties of the Tunnel Diode

Simply stated, a tunnel diode is a heavily doped p-n semiconductor junction. A lightly doped junction has little resistance when forward biased and high resistance when reverse biased up to the reverse breakdown or Zener voltage. If the concentration of impurity atoms is increased, the reverse breakdown voltage approaches zero; and it might be thought that an infinite concentration of impurity atoms would be needed to attain a breakdown condition at zero applied voltage; however when doping is increased beyond a definite concentration, which is easily obtainable in practice, a reverse breakdown condition exists even at a small forward bias, and the device is a tunnel diode. Such a diode exhibits negative resistance at a small forward bias.

The static characteristic curve of a tunnel diode is shown in Plate I. The negative resistance region is between the peak point, labeled b, and the valley point, labeled d; and point c is called the forward point. Theoretically this curve should be the sum of a Gaussian and an exponential,<sup>22</sup>

but it differs in two ways. First, the current in the valley region is always greater than would be expected, the difference being due to defect states in the forbidden gap energy band as postulated by Yajima and Esaki.<sup>8</sup> Second, the peak region is always skewed slightly to the right, this being attributed to stray circuit parameters which can never be completely eliminated.

In order to make circuit calculations, the characteristic curve may be approximated by two parabolas<sup>29,44</sup> or a series of straight lines.<sup>22</sup> In the latter approximation the resistance in the low voltage region is given by the formula  $R_{d1} = 0.75 V_p / I_p$ , where  $V_p$  is the peak voltage and  $I_p$  is the peak current; and the resistance in the high voltage region is given by  $R_{d2} = (V_{fp} - V'_v) / (I_p - I_v)$ , where  $V_{fp}$  is the forward point voltage,  $I_v$  is the valley current, and  $V'_v = 0.5(V_{fp} - V_v)$  with  $V_v$  being the valley voltage. The peak, valley, and forward point voltages, which are determined by the semiconductor material, are 55 mV, 359 mV, and 500 mV respectively at 25° C for germanium and about double these values for gallium arsenide tunnel diodes.<sup>21</sup> Measured values of parameters usually agree with those calculated from the linearized curve to within ten per cent.

The peak current is determined by the impurity concentration and the cross-sectional area of the junction. In practice the junction is made larger than necessary and then etched away until the desired current is achieved. A rather

high current density is used to decrease the capacitance, which depends on the peak current. A one milliamperere unit, for example, might have a junction diameter of less than  $3 \times 10^{-4}$  inch. The ratio of peak current to junction capacitance,  $I_p/C$ , is approximately constant for a given semiconductor material and doping, and is about 1/2 for the 1N3118 gallium arsenide and about 5 for the germanium tunnel diodes utilized in our circuit. Because an input pulse must supply charge to the junction capacitance, and because the rate of charge accumulation is a function of overdrive, there is a time delay in the firing of the tunnel diode. The variation in this time delay with overdrive is called the slewing characteristic. The time delay at the input stage is reduced considerably by using a germanium tunnel diode, for which the junction capacitance is about ten times smaller than that of the gallium arsenide tunnel diode.

## 2. The Univibrator Circuit

There are several possible variations of the basic tunnel diode univibrator shown in Plate II: Sometimes the bias voltage is introduced on the other side of the inductor; occasionally there is a resistor between the tunnel diode and ground, and quite often all polarities are reversed. A typical output pulse is shown in Plate III with the letters a, b, c, d, and o corresponding to the same letters in Plate I. The voltage and current under quiescent conditions are given by the coordinates of point o in Plate I. The negative

resistance region between b and d is unstable; consequently the tunnel diode switches rapidly to point c to accommodate the input current, thus producing the leading edge of the output pulse. More precisely, the current may rise above c for large input pulses. The curve is then followed from c to d, thus producing the corresponding portion of the output pulse, whereupon the circuit relaxes to the operating point, o. The wiggles in the tail of the pulse are due to reflections within the circuit and oscillations about the operating point.

The maximum voltage (or current) to which a pulse rises is the pulse height. If the initial slope of the pulse is small, and the top of the pulse is fairly flat, it may be difficult to measure exactly when the pulse starts and when it reaches its maximum. For these reasons the rise time,  $t_r$ , of a pulse is defined as the time for the pulse to rise from 10% to 90% of the pulse height. If a trigger of minimal amplitude is used with a constant current bias source, for which the load line is horizontal, the rise time of a tunnel diode is approximately given by the relation  $t_r = (V_{fp} - V_p)C / (I_p - I_v)$ , where all quantities have been defined previously. The switching time, which is determined mainly by the junction capacitance and somewhat by the amount of charge available from the trigger, of a GaAs tunnel diode with a peak current of 10 ma and a junction capacitance of 10 pfd is reported to be approximately one nanosecond,<sup>25</sup> and this was verified on a Tektronix Tunnel Diode Risetime Tester. With

the tunnel diode connected into a univibrator circuit, the risetime of an output pulse is somewhat greater, typically around two nanoseconds or less.

In a manner similar to the above, the decay time,  $t_d$ , is defined as the time for the pulse to decay from 90% to 10% of the pulse height. The pulse width is the full width of the pulse at half maximum, FWHM. Because the circuit is underdamped, the pulse overshoots equilibrium during decay, and the recovery time includes this overshoot. The minimum time between two input pulses which will cause the univibrator to be triggered twice when the second pulse is 10% above threshold is the pulse pair resolution time,  $t_p$ . In the simple tunnel diode univibrator the expression  $t_p = 14(\text{FWHM})$  is valid over a fairly large range.<sup>47</sup> Whetstone has shown that by replacing the 13 ohm load resistor with a high conductance diode and resistor combination, the recovery time of the circuit can be controlled so that pulse pairs well under ten nanoseconds apart can be counted, but the simpler circuit was considered adequate for our purpose.

The output pulse height is a function of the inductance in the circuit. Results from four units, which are plotted in Plate IV, differ from those obtained by Whetstone<sup>48</sup> for several reasons. The pulse height was measured not across the tunnel diode itself but at the point where the pulse entered the coincidence circuit; therefore the pulse heights were smaller than those of Whetstone. The inductance was somewhat difficult

to measure due to its small magnitude. The inductance plotted is that of the inductor, as measured with a Tektronix 130 L-C Meter, and does not include the stray inductance. The output pulse height also varies with the input pulse height, and is some constant plus about 5% of the input pulse height. This dependence is greatly reduced by feeding the output from the first univibrator to a second univibrator to produce a standardized pulse which is almost independent of the input pulse height. Over a range of several volts the variation in pulse heights from a two stage unit was just barely perceptible on a Tektronix sampling scope. There is another advantage in using a two stage unit. For a wide input pulse the first stage may produce a train of pulses, but with careful adjustment of the bias on the second stage, it will fire on only the first pulse in the train due to the fact that the first pulse of the train has the greatest pulse height.

A complete circuit as shown in Plate VI has two discriminator units, each with two tunnel diodes, and a coincidence unit with two tunnel diodes. The inductor in the final univibrator has been chosen larger than any of the other inductances so that the final output pulse is wide enough to be accepted by succeeding equipment. Through the complete circuit there is a propagation time which measures about eight nanoseconds but depends on the bias settings. The bias on any univibrator stage must be set low enough so that a pulse from the previous stage will trigger it but high enough so that

feedback pulses from succeeding stages will have no effect.

Of the several input circuits tested, it was difficult to ascertain which one was really best since all were able to fire the univibrator. Because of the threshold nature of the circuit, the univibrator either fires or does not fire, so simply looking at the output does not give a measure of the quality of the input circuit. A transistor input circuit was constructed which ultimately gave good results, but as there were some difficulties in getting the bias voltages for the transistor initially adjusted, and as the amplification properties of the transistor were not needed, this circuit was regarded as producing unnecessary complications. Pulse transformers constructed from ferrite cores according to information obtained from Whetstone were used in the input circuit and gave acceptable results, but perhaps due to the use of wide input pulses, slightly greater input pulse heights were required. A simple capacitor input circuit was also tested and gave good results with capacitances from 33  $\mu\text{F}$  to 100 times this value.

### 3. Detection of Coincident Pulses

Consider two standard pulses, identical except for time of occurrence, which are added linearly and fed to a coincidence circuit. Because the coincidence circuit is set so as not to trigger on a single pulse height, it will not trigger unless the pulses overlap and the sum of the overlapping pulses at some time is greater than the single pulse height.

This can occur only if the pulses are coincident to within a time of less than the FWHM of a single pulse. In practice the coincidence circuit must be set to trigger at a threshold greater than once but less than twice a single pulse height. The same principle can also be used to determine if three or more pulses are coincident within a certain time interval.<sup>11</sup> Other methods of time analysis than that of pulse overlap are sometimes used.<sup>9</sup>

To measure the resolving time a series of 50 ohm cables of different lengths were made and the time for a pulse to propagate through each was measured with a Tektronix sampling scope. A single source fed the inputs of the coincidence circuit through different cable lengths. By selection of the cables it was determined that the resolving time of the circuit in a typical configuration was between 2.5 and 3 nano-seconds, which was consistent with the standard pulse widths.

#### 4. Zero Crossover

Complications arise from the statistical nature of photomultiplier pulses, the problem being especially acute in the case of slow pulses from NaI(Tl) detectors.<sup>43</sup> The question arises as to which part of the photomultiplier pulse gives the best time measurement. When a quantum of radiation strikes the cathode, a photoelectron is ejected. The electron is accelerated to the first dynode where more electrons are ejected, and so on. Since the electrodes have finite dimensions, the paths of different electrons vary slightly in length,

and the final anode collects a swarm of electrons which arrive within some interval of time.

The trailing edge of the pulse is highly dependent on the circuit and is not useful for timing purposes. The leading edge of the photomultiplier pulse tells only when the first few electrons arrive at the anode, but we seek the average time of arrival, which is approximately at the time of the maximum height of the pulse. As the top of the pulse may be fairly flat, the time at which it reaches a maximum may be difficult to ascertain. The negative photomultiplier pulse can be differentiated thus producing a pulse which is initially negative going and then positive going. If the differentiating circuit is properly designed, the zero crossover between the negative and positive going parts of the differentiated pulse will be a good measure of the time of the maximum of the photomultiplier pulse. The zero crossover signal may also be obtained by the clipping stub method or the LC tank circuit method. Some circuits are so sensitive that they can detect a single photoelectron. In practice our coincidence circuit does not respond at exactly the zero crossover but very soon afterwards.

#### 5. Noise and Feedthrough

With a single input signal of 100 mV the feedthrough at the output of the second stage is 0.8 mV, while a single 500 mV signal gave a feedthrough of 1 mV. Noise generated in the circuit was certainly less than 1 mV. Since the output pulse for coincident singles had a height of several hundred millivolts,

noise and feedthrough were negligible and did not upset succeeding circuits.

An important consideration is the amount of noise and feedthrough at the coincidence diode. A 100 mV signal at the input produced a signal of 2 mV at the coincidence diode due to noise and feedthrough, and varied almost linearly with increasing input signal. As a smaller input signal produced smaller feedthrough, and as the standard pulse had a fixed height, it appeared best to use the least amount of amplification needed before applying the signal to the first tunnel diode. The effect of large signals was to increase the resolving time of the circuit. The circuit operated most effectively when the input signal was not too much above threshold, say 30% at most. For very severe overdrive the coincidence diode might be expected to fire on a single pulse. With the circuit set to give an output pulse for coincident 100 mV pulses, a single input pulse of 20 volts would not fire the coincidence diode.

During one period of counting it was found that many spurious pulses were registering on the scaler at odd intervals. While observing the scaler it was determined that these pulses always occurred when an electric desk calculator was being used in the same room. Thus the circuit was not adequately shielded from line transients.

## 6. Slewing

The "slewing" or "walking" characteristic is defined as

the time variation of the output pulse as a function of excess of the input pulse over threshold.<sup>46</sup> The threshold must be set at a few millivolts above zero, otherwise the circuit will oscillate. For this reason the circuit can never really trigger at the zero crossover but will trigger a very short time afterward when the signal has risen to threshold. As the amplitude of the input signal is increased, the slope at the zero crossover increases; because the signal reaches threshold sooner, the tunnel diode would be expected to fire sooner. This is the case for a positive pulse, but for a zero crossover pulse another factor comes into play. The negative portion of the pulse drives the operating point of the tunnel diode down the positive resistance part of the characteristic curve, and it would seemingly take longer for the current to rise to the peak point. Thus there are two competing effects. The greater slope of a higher amplitude input pulse tends to make the tunnel diode fire sooner, while the larger negative portion of the input pulse drives the tunnel diode down from the operating point and tends to make the tunnel diode fire later. The result is a U-shaped slewing characteristic as the tunnel diode fires late for both small and large zero crossover input pulses. Plate VIII shows the slewing characteristic as a function of per cent of threshold. The slewing characteristic of a commercial tunnel diode coincidence circuit is shown in Plates XI and XII. These results are not quite as good as those which have been reported,<sup>46</sup> even though we used a germanium

rather than a gallium arsenide tunnel diode at the input stage to improve the slewing characteristic.

### 7. Effect of Temperature

At higher temperatures the effect of intrinsic carrier concentration, the result of thermally created electron-hole pairs, becomes large in comparison to the effect of impurity atoms. In the tunnel diode this results in a changing of both the peak current and the peak voltage. In a germanium tunnel diode the decrease in peak voltage with increasing temperature is about  $0.11 \text{ mV/C}^\circ$ . In our circuit the tunnel diodes were mounted in a position which allowed adequate ventilation to reduce temperature changes to a negligible amount.

### 8. Jitter

The jitter of the threshold on the input stage is approximately 2 mV for the germanium tunnel diode. The minimum usable threshold without sacrificing stability is approximately 60 mV, but usually the threshold voltage is set at 100 mV or higher. The jitter of the threshold voltage results in a time jitter of the firing of the tunnel diode. This time jitter was determined to be a small fraction of a nanosecond, and for the present equipment is small enough to neglect.

### 9. Nanosecond Systems, Inc., Equipment

In the fall of 1964 equipment was purchased from Nanosecond Systems, Inc. The circuit employed is that of Whetstone<sup>48</sup>

with improvements.<sup>47</sup> It was found to behave quite similarly to the previously constructed equipment. It possessed many of the same difficulties such as double pulsing on wide input pulses. One good feature was that the commercial equipment was much better shielded and did not respond to line transients from the previously troublesome electric desk calculator.

The resolving time of the Nanosecond circuit was measured in two different ways for various settings of the knob labeled "logic" on the coincidence unit. Table I shows the data obtained by feeding signals from a pulser to two discriminators through different delay lines. The range in time over which one signal could be varied relative to the other was then taken as twice the resolving time of the circuit. As a check the linear sum of the two standard 410 mV pulses entering the coincidence circuit was also viewed on the sampling oscilloscope. Table II shows the maximum height of this sum with

Table I. Resolving time by the direct delay method.

Logic knob setting	Resolving time in nanoseconds
3.60	16.3
4.00	14.5
5.50	5.5
7.00	2.0
7.50	.75

various delays in the circuit. The logic knob on the coincidence unit is actually a threshold setting knob although it is

not directly marked in millivolts. Suppose a particular setting of the logic knob, say 5.00, corresponds to a threshold of 610 mV. From Table II we see that one pulse could be varied in relative time from 28 to 48 nsec, which would give a resolving time of 10 nsec. The resolving time at various logic setting was also determined by the chance coincidence method from the data in Table III. The right hand column was calculated from the formula  $t = N_c / (2 N_1 N_2)$ , where  $N_1$  and  $N_2$  are the single counting rates and  $N_c$  is the chance coincidence counting rate. As shown by the plot in Plate IX the results of the two methods are in excellent agreement.

Table II. Maximum height of two overlapping standard pulses.

Delay between pulses in nanoseconds	Maximum height in millivolts
10	410
16	420
20	510
28	610
30	660
36	810
40	790
48	610
50	550
56	420
60	410

Table III. Resolving time by the chance coincidence method.

Logic setting	Coin. counts	Counting time	Count rate from $Co^{60}$ (cpm)	Count rate from pulser (cpm)	Resolving time (nsec)
3.60	1684	30.00 min	204 217	251 682	16.5
4.00	660	30.00 min	204 217	251 592	12.9
5.50	312	30.00 min	205 277	251 587	6.1
7.00	1423	12.00 hr	203 783	251 205	1.15
7.50	801	17.75 hr	205 458	251 789	0.435

### III. THEORY OF DIRECTIONAL CORRELATION

#### 1. The Directional Correlation Function

Directional correlation measurements involve the coincidence counting rate as a function of the angle between the propagation vectors of two cascade radiations. Many treatments of the subject are found in the literature, but we will give only a brief discussion of the theory since this paper is mainly concerned with the experimental problems.

For convenience we take the direction of propagation of the first gamma ray as the polar axis of spherical polar coordinates. The angular distribution can be most appropriately described by a series of spherical harmonics:

$$W(\theta, \varphi) = \sum_{L,m} a_{Lm} Y_L^m(\theta, \varphi), \quad (1)$$

where  $W(\theta, \varphi)$  is proportional to the coincidence counting rate as a function of the direction of propagation of the second gamma ray.

For randomly oriented nuclei and the special polar axis

we observe that the distribution must be independent of the azimuth angle. In this case  $m=0$ , and the series may be simplified:

$$W(\theta, \phi) = \sum_L a_{L0} Y_L^0(\theta, \phi) = W(\theta)$$

$$W(\theta) = \sum_L A_L P_L(\cos \theta) \quad (2)$$

where  $\theta$  is the angle between the propagation vectors. A general derivation with an arbitrary orientation of the coordinate system gives the same result.

Two more simplifications can be made. If the transitions involve states of definite parity, only the even Legendre polynomials appear. Since the transitions are between eigenstates of angular momentum, the maximum value of  $L$  is limited by certain triangular inequalities:

$$L/2 = \text{Min}(L_1, I, L_2) \quad (3)$$

where  $L_1$  and  $L_2$  are the angular momenta of the radiations and  $I$  is the angular momentum of the intermediate state.

Of course this series could be expressed in terms of another set of functions such as powers of  $\cos \theta$ , but a particular advantage of Legendre polynomials is that each coefficient can be split into two factors, each of which depends on only one of the transitions. For pure transitions,

$$A_L = F_L(L_1, L_1, I_i, I) F_L(L_2, L_2, I_f, I) \quad (4)$$

where  $I_i$  and  $I_f$  are the angular momenta of the initial and final states. These factors are certain combinations of

Clebsch-Gordon and Racah coefficients and have been tabulated in various references.<sup>6</sup> Note that  $W(\theta)$  is symmetric with respect to an interchange of the order of the transitions. If a transition is mixed with a mixing ratio,  $d$ , defined by

$$d^2 = \frac{\text{intensity of } (L+1)}{\text{intensity of } (L)}, \quad (5)$$

then the factors become

$$F_L(L_1, L_1+1, I_1 I) = \frac{F_L(L_1, L_1, I_1 I) + 2dF_L(L_1, L_1+1, I_1 I) + d^2 F_L(L_1+1, L_1+1, I_1 I)}{1 + d^2} \quad (6)$$

We now derive these functions for gamma-gamma angular correlation in a more explicit but less useful form. Initially a nucleus may be in any of the  $2I_1 + 1$  equally populated initial substates with spin  $I_1$  and projection quantum number  $M_1$ . The first gamma ray is characterized by quantum numbers  $L_1$  and  $M_1$ . For the special choice of polar axis  $M_1$  can be only  $+1$  or  $-1$ . The intermediate state is characterized by  $I$  and  $M$ . These three sets of quantum numbers must satisfy the vector addition

$$\overline{(I_1 M_1)} = \overline{(L_1 M_1)} + \overline{(I M)} \quad (7)$$

From the definition of Clebsch-Gordon coefficients

$$|I_1 M_1\rangle = \sum_{M, M_1} \langle IL_1 MM_1 | I_1 M_1 \rangle |IM\rangle |L_1 M_1\rangle. \quad (8)$$

Thus the relative transition probabilities are given by

$$(\langle IL_1 MM_1 | I_1 M_1 \rangle)^2 \quad (9)$$

and the relative populations of the intermediate substates are

$$\sum_{M_1} (I_{L_1 M_1} I_{i M_i})^2 \quad (10)$$

where we have summed incoherently since the phases are random, and the prime indicates that  $M_1$  is only +1 or -1. The angular distribution of the first gamma ray is then

$$\sum_{M, M_1} (I_{L_1 M M_1} I_{i M_i})^2 F_{L_1}^{M_1}(\theta) \quad (11)$$

where  $F_{L_1}^{M_1}(\theta)$  is some angular function characteristic of the radiation. For a radiating multipole of order  $L$  and projection  $M$

$$F_L^M(\theta) = \frac{[L(L+1)-M(M-1)] |Y_L^{M-1}|^2 + 2M^2 |Y_L^M|^2 + [L(L+1)-M(M+1)] |Y_L^{M+1}|^2}{2L(L+1)} \quad (12)$$

Since the first gamma ray is observed only at  $\theta=0$ , the correlation function is

$$W(\theta) = \sum_{M_i, M_f, M_1} (I_{L_1 M M_1} I_{i M_i})^2 F_{L_1}^{M_1}(\theta) (I_{f L_2 M_f M_2} I_{M})^2 F_{L_2}^{M_2}(\theta)$$

$M_1 = +1 \text{ or } -1$

$M_2 = M_f - M$  (13)

## 2. The Ni<sup>60</sup> Cascade

The standard nucleus for directional correlation measurement is Ni<sup>60</sup>. The nucleus Co<sup>60</sup> decays to Ni<sup>60</sup> by negatron emission with end point energies of 0.313 Mev and 1.45 Mev with very nearly 100% of the transitions having the former end

point energy. These transitions lead to a  $\text{Ni}^{60}$  nucleus in a 2.5 Mev excited state as shown in Plate XIII. The ground state is reached by emission of two cascade gamma rays of energies 1.17 Mev and 1.33 Mev. The 1.33 Mev gamma ray has been established as the second transition by means of nuclear fluorescence resonance experiments. The spin sequence is well established as  $4(E2)2(E2)0$  with both transitions being pure electric quadrupole. All three levels have positive parity. The theoretical directional correlation function for the  $\text{Ni}^{60}$  cascade assuming the above spin sequence is

$$W(\theta) = 1 + 0.102 P_2(\cos \theta) + 0.0091 P_4(\cos \theta). \quad (14)$$

### 3. Analysis of Chance Rates

Before comparing experimental data with the theory previously described, several corrections must be made. We must first subtract chance coincidences between unrelated pulses. The analysis of chance coincidences is treated extensively in the literature.<sup>27,34,39,40</sup>

In a double coincidence circuit the chance coincidence rate is easily shown to be

$$N_c = 2 t(N_1 - N_t)(N_2 - N_t) \quad (15)$$

where  $t$  is the resolving time,  $N_t$  is the true coincidence rate, and  $N_1$  and  $N_2$  are the singles counting rates in the two channels. In practice the true coincidence rate is always so very much smaller than the singles counting rates that the  $N_t$  terms may be neglected.

In a triple coincidence circuit of the fast-slow type

there are several possibilities for chance counts. The various singles and coincidence rates are shown in Figure 1. It is assumed that the singles rates,  $N_I$  and  $N_{II}$ , from the fast discriminators are larger than the corresponding singles rates,  $N_1$  and  $N_2$ , from the single channel analyzers.

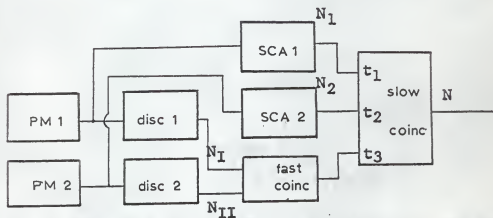


Fig. 1. Block diagram of a fast-slow coincidence circuit.

For simplicity it is assumed that the coincidence circuits operate in the following manner. A single pulse input to the fast circuit produces a rectangular pulse of width  $t_f$ . If two pulses from the two fast inputs overlap at any time, an output pulse is produced. The slow circuit works in a similar manner except that pulses from all three inputs must overlap at some time in order to produce an output pulse.

The chance coincidence rate between  $N_1$  and  $N_2$  only is given by

$$N(1 \& 2) = (t_1 + t_2)N_1N_2 \quad (16)$$

with an average overlap time of  $t_1t_2/(t_1 + t_2)$ . The triple chance coincidence rate is then

$$\begin{aligned} N_c(1\&2\&3) &= (t_3 + \frac{t_1t_2}{t_1 + t_2})(t_1 + t_2)N_1N_2N_3 \\ &= (t_1t_2 + t_1t_3 + t_2t_3)N_1N_2N_3 \end{aligned} \quad (17)$$

For  $t_1 = t_2 = t_3 = t$ , the preceding expression is

$$N_c(1\&2\&3) = 3t^2 N_1N_2N_3 \quad (18)$$

The fast coincidence rate,  $N_3$ , can be split into several parts:

$$N_3 = N_t + N_{f1} + N_{f2} + N_f + 2t_f N_I N_{II} \quad (19)$$

where  $N_t$  is the true coincidence rate between gamma rays of the proper energies,  $N_{f1}$  is the fast coincidence rate where only the first gamma rays have the proper energy,  $N_{f2}$  is the rate with only the second gamma rays having the proper energy,  $N_f$  is the fast coincidence rate between gamma rays, neither of which has the proper energy, and the last term in (19) is the chance coincidence rate.

The triple slow coincidence rate,  $N$ , can be divided into eight parts:

$$\begin{aligned} N &= N_{f1}2 + N_{f1}(2) + N_f(1)2 + N_f(1)(2) + N(f)12 + N(f)1(2) \\ &\quad + N(f)(1)2 + N(f)(1)(2) \end{aligned} \quad (20)$$

where parentheses indicate a component which is in slow coincidence but not fast coincidence with the other components.

As an example  $N_{f1}(2)$  is the coincidence rate between  $N_{f1}$  and a gamma ray of energy  $E_2$ , the latter being in slow but not

fast coincidence with the former. The nature of the various terms is easily deduced from the following formulas:

$$N_{f1}(2) = 2 t N_{f1} N_2 \quad (21)$$

$$N_f(1)2 = 2 t N_{f2} N_1 \quad (22)$$

$$N_f(1)(2) = 3 t^2 N_1 N_2 N_f \quad (23)$$

$$N_{(f)1}(2) = (2 t_f N_{II} N_I) 2 t N_2 \quad (24)$$

$$N_{(f)}(1)2 = (2 t_f N_I N_2) 2 t N_1 \quad (25)$$

$$N_{(f)}(1)(2) = 3 t^2 N_1 N_2 2 t_f N_I N_{II} \quad (26)$$

Equation (20) now becomes

$$\begin{aligned} N = N_t + 2 t (N_{f1} N_2 + N_{f2} N_1) + 3 t^2 N_1 N_2 N_f + 2 t_f N_1 N_2 \\ + 4 t_f t N_1 N_2 (N_I + N_{II}) + 6 t^2 t_f N_1 N_2 N_I N_{II}. \end{aligned} \quad (27)$$

#### 4. Experimental Considerations

The singles counting rate in either detector is

$$N_i = M p_i e_i \Omega_i \quad (28)$$

where  $M$  is the source strength in disintegrations per unit time,  $p_i$  is the probability that a disintegration will lead to the gamma ray of interest,  $e_i$  is the efficiency of the detector, and  $\Omega_i$  is the solid angle subtended by the detector in units of  $4\pi$ . The accidental or chance counting rate in the coincidence circuit is

$$\begin{aligned} N_c = 2 t e_c N_1 N_2 \\ = 2 t e_c M p_1 e_1 \Omega_1 M p_2 e_2 \Omega_2 \end{aligned} \quad (29)$$

where  $e_c$  is the efficiency of the coincidence circuit. The

true coincidence rate is

$$N_t = M p_1 p_2 e_1 e_2 e_c \Omega_1 \Omega_2 K(\theta) \quad (30)$$

where  $K(\theta)$  is proportional to the directional correlation function and has an average value of unity. The true to chance ratio at any angle is

$$\frac{N_t}{N_c} = \frac{M p_1 p_2 e_1 e_2 \Omega_1 \Omega_2 K(\theta)}{2 t e_c M p_1 e_1 \Omega_1 M p_2 e_2 \Omega_2} \quad (31)$$

so that the average value is

$$(N_t/N_c)_{ave} = 1/(2 t_f M). \quad (32)$$

The actual counting rate is the sum of the true and chance rates from which the chance rate must be subtracted. In order for the chance rate to contribute only a small error to the results the true to chance rate should be as high as possible. In practice there is a lower limit for the resolving time of the coincidence circuit due to electronics. Furthermore if  $M$  is small, the counting rate will also be small, but it is desirable to have the singles rates many orders of magnitude above the background rate. A good compromise is to have the true to chance rate between five and twenty.

As a numerical example, let  $N_t/N_c = 5$  and  $t_f = 25$  nsec. Then from (32)

$$M = N_c / (2 t_f N_t) = 0.1 \text{ mc} \quad (33)$$

Also, let  $e_1 = e_2 = 0.03$ ,  $\Omega_1 = \Omega_2 = 0.01$ , and  $e_c = 1$ . From (29) and (30)

$$\begin{aligned} N_c &= 4.3/\text{min} \\ N_t &= 21.5/\text{min} \end{aligned} \quad (34)$$

Suppose we wish to know the counting rate to within the fractional statistical error  $E$ , and there is no error in the time  $T$ .

$$E^2 = (N_{t+c} + N_c) / (N_t^2 T)$$

$$T = (N_{t+c} + N_c) / (N_t E)^2 \quad (35)$$

For  $E = 1\%$ ,  $T = 600$  min at each angle. For  $E = 9.1\%$ , then  $T = 60\,000$  min at each angle. As will be shown in the next section, for counters which subtend a finite solid angle, the directional correlation function is attenuated. For this example

$$\bar{W}(\theta) = 1 + 0.100 P_2(\cos \theta) + 0.0086 P_4(\cos \theta) \quad (36)$$

with a few values being

$$\bar{W}(90^\circ) = 0.9532$$

$$\bar{W}(135^\circ) = 1.0215$$

$$\bar{W}(180^\circ) = 1.1086 \quad (37)$$

In order to propagate the errors we need White's matrix:

$$\frac{1}{105} \begin{pmatrix} 42 & 56 & 7 \\ -90 & 40 & 50 \\ 48 & -96 & 48 \end{pmatrix} \begin{pmatrix} N(90^\circ) \\ N(135^\circ) \\ N(180^\circ) \end{pmatrix} = \begin{pmatrix} A_0 \\ A_2 \\ A_4 \end{pmatrix} \quad (38)$$

Suppose we wish to determine  $A_4$  to within ten per cent, then from (38) the counting rate of true coincidences at each angle must be about 0.15% correct. From (35) the counting time at each angle is twenty days! If both counters accept both gamma rays, only half this time is required. We see that a tremendous amount of time is required to collect directional

correlation data.

### 5. Correction for Finite-Size Detectors

When the directional correlation is observed experimentally, it appears "smeared out" according to

$$\bar{W}(\theta) = \frac{\iint d\Omega_1 d\Omega_2 e_1 e_2 W(\theta')}{\iint d\Omega_1 d\Omega_2 e_1 e_2} \quad (39)$$

The efficiency,  $e$ , of a detector has been treated in several ways. Feingold and Frankel<sup>17</sup> use an expansion in spherical harmonics for the efficiency of an arbitrary detector

$$e(\theta, \phi) = \sum_{L,m} \left( \frac{2L+1}{4\pi} \right)^{1/2} a_{Lm} Y_L^m(\theta, \phi) \quad (40)$$

For a circularly symmetric detector as shown in Figure 2, this expression simplifies since  $e$  is independent of  $\phi$ .

$$e(\theta) = \sum_L a_L P_L(\cos \theta) \quad (41)$$

The expression which Rose<sup>37</sup> uses for the efficiency is  $e = 1 - \exp(-kx)$ , where  $k$  is the absorption coefficient for the gamma ray energy of interest and  $x$  is the detector thickness at the angle of incidence of the gamma ray. For a circularly symmetric detector

$$\begin{aligned} x &= t \sec b \quad \text{for } 0 \leq b \leq \tan^{-1} [r/(h+t)] = b' \\ x &= r \csc b - h \sec b \quad \text{for } b' \leq b \leq \tan^{-1}(r/h) \end{aligned} \quad (42)$$

Since the directional correlation function is most often expressed as a series of Legendre polynomials, we must perform

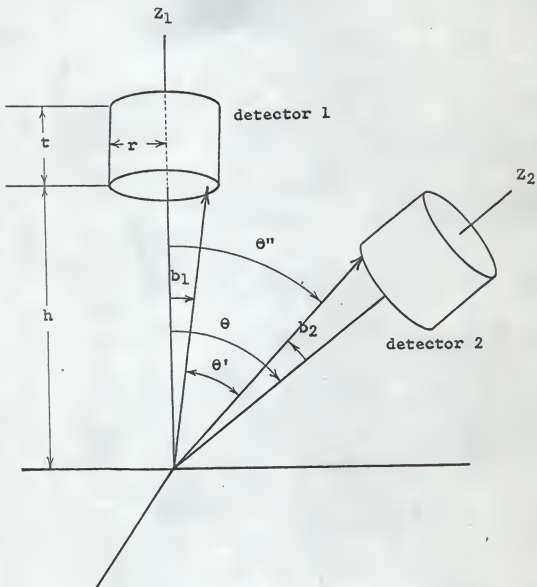


Figure 2. Angles involved in correction for finite-size detectors.

integrations of the form

$$I = \iint d\Omega_1 d\Omega_2 e_1 e_2 P_L(\cos \theta'). \quad (43)$$

We express  $P_L(\cos \theta')$  in terms of  $b_1$  and  $\theta''$  by means of the addition theorem for spherical harmonics.

$$P_L(\cos \theta') = \frac{4\pi}{2L+1} \sum_{m=-L}^{+L} Y_L^{m*}(b_1, \vartheta) Y_L^m(\theta'', \vartheta'') \quad (44)$$

Let  $x_1$  be independent of  $\vartheta_1$  so that only terms with  $m=0$  contribute to the integral. Then

$$P_L(\cos \theta') = \frac{4\pi}{2L+1} Y_L^0(b_1, \vartheta) Y_L^0(\theta'', \vartheta'') + \dots$$

$$P_L(\cos \theta') = P_L(\cos b_1) P_L(\cos \theta'') + \dots, \quad (45)$$

and the integral  $I$  becomes

$$0 \int_0^{2\pi} d\vartheta_1 \int \sin b_1 db_1 P_L(\cos b_1) e_1 \iint d\vartheta_2 \sin \theta'' d\theta'' P_L(\cos \theta'') e_2 \quad (46)$$

The efficiency of the second detector is most easily expressed in terms of angles measured from the  $Z_2$  axis. We apply a rotation matrix and drop the  $m=0$  terms which do not contribute.

This gives

$$P_L(\cos \theta'') = D_{00}^L(0, \theta, 0) P_L(\cos b_2) + \dots$$

$$= P_L(\cos \theta) P_L(\cos b_2) + \dots$$

The integral  $I$  becomes

$$I = 4\pi^2 J_L(1) J_L(2) P_L(\cos \theta),$$

where

$$\begin{aligned} J_L(1) &= \int \sin b_1 db_1 P_L(\cos b_1) e_1 \\ J_L(2) &= \int \sin b_2 db_2 P_L(\cos b_2) e_2. \end{aligned} \quad (47)$$

The experimentally observed directional correlation function then becomes

$$\bar{W}(\theta) = 1 + Q_{22} A_2 P_2(\cos \theta) + Q_{44} A_4 P_4(\cos \theta) + \dots,$$

where

$$\begin{aligned} Q_{22} &= Q_2(1) Q_2(2) \\ Q_2(1) &= J_2(1) / J_0(1). \end{aligned} \quad (48)$$

As an approximation we assume that  $e$  is constant up to  $b_0$  and zero thereafter.

$$\begin{aligned} J_L &= \int_0^{b_0} P_L(\cos b) e \sin b db \\ J_0 &= e \int \sin b db = e(1 - \cos b_0) \\ J_2 &= e \int P_2(\cos b) \sin b db = e \cos b_0 (1 - \cos^2 b_0)/2 \\ J_4 &= e \int P_4(\cos b) \sin b db \\ &= e \cos b_0 (1 - \cos^2 b_0)(7 \cos^2 b_0 - 3)/8 \end{aligned} \quad (49)$$

Then the attenuation factors for similar detectors are

$$\begin{aligned} Q_{22} &= (Q_2)^2 \\ Q_2 &= \cos b_0 (1 + \cos b_0)/2 \\ Q_{44} &= (Q_4)^2 \\ Q_4 &= \cos b_0 (1 + \cos b_0)(7 \cos^2 b_0 - 3)/8 \\ b_0 &= \tan^{-1}(r/h). \end{aligned} \quad (50)$$

These are the formulas given by Frauenfelder and Steffen.<sup>18</sup>

As pointed out by Lawson and Frauenfelder,<sup>32</sup> the attenuated directional correlation function is of the form derived above only for centered point sources and circularly symmetric detectors. Otherwise a mixing of the different  $A_L$  terms occurs.

#### IV. MEASUREMENT OF THE Ni<sup>60</sup> DIRECTIONAL CORRELATION

##### 1. Apparatus

A source, roughly of strength 0.1 mc as will be shown later, was prepared by evaporating a Co Cl<sub>2</sub> solution inside a carbon cylinder of outside diameter 3/16 inch and inside diameter 3/32 inch. The wall of the carbon cylinder constituted an absorber of 0.375 gm/cm<sup>2</sup>, which was more than sufficient to absorb all the beta particles from the 0.313 MeV beta decay, for which only 0.086 gm/cm<sup>2</sup> was needed. The total absorbing material consisting of the cylinder wall and the cover on the NaI crystal was not quite enough to absorb completely all beta particles from the 1.48 MeV beta decay, which would have required 0.7 gm/cm<sup>2</sup>, but no additional absorber was introduced since this decay is only 0.01% as intense as the 0.313 MeV decay.

The fixed detector was a NaI(Tl) scintillation crystal 2 inches by 5 cm thick placed 9.2 cm from the source, and the movable detector was a NaI(Tl) crystal 1 3/4 inches by 3 cm thick placed 8.4 cm from the source. Availability was the

only reason for choosing different sized crystals. Each crystal was mounted on an RCA 6342 photomultiplier tube operated at 1100 volts and placed on a specially constructed circular table with the source at the center. Each crystal was surrounded by a very thick conical lead shield.

Fast coincidences between pulses from the photomultipliers were detected in the Nanosecond Systems equipment and fed to a triple slow coincidence unit built by David Draeger.<sup>14</sup> Photomultiplier pulses were also directed through a Nuclear Data 500 dual single channel analyzer to the slow coincidence unit. The fast-slow coincidences were counted on a scaler. Simultaneously singles counts passing through the Nuclear Data 500 analyzers were counted on scalars.

## 2. Determination of Resolving Times

A 1.5 uH inductor was placed in the fast coincidence logic circuit. The resolving time of the fast circuit was determined by the chance coincidence method. Two rather long runs were taken giving the following:

$$N_I = 64\,927\,808 / 836 \text{ min}$$

$$N_{II} = 18\,187\,418 / 836 \text{ min}$$

$$N_C = 1203 / 836 \text{ min.}$$

Using (15) the resolving time of the fast circuit is

$$t_f = N_C / (2 N_I N_{II}) = 24.3 \pm .7 \text{ nsec.}$$

The logic setting used was 3.70. Note that the graph in Plate IX cannot be used here because the inductors were not of

the same value, but from Plate IX and the graph of Plate V, we can conclude that the result is entirely consistent with previous measurements. This resolving time will be used to calculate expected chance rates.

The resolving time of the slow coincidence unit was determined by the same method.

$$N_1 = 303\ 348 / 5 \text{ min}$$

$$N_2 = 94\ 612 / 5 \text{ min}$$

$$N_c = 307 / 5 \text{ min}$$

The resolving time of the slow unit was then

$$t = 1.60 \pm .09 \text{ usec.}$$

This was consistent with oscilloscope observations of the waveforms in the circuit which showed the pulses fed to the slow coincidence unit to be about 1.5 usec wide.

### 3. Determination of Chance Rates

The measured true plus chance slow coincidence rate between  $N_1$  and  $N_2$  was about 105 cpm of which 91 cpm was the expected chance coincidence rate and  $74 \pm 8$  was the measured chance rate. The measured true plus chance fast coincidence rate between  $N_I$  and  $N_{II}$  was about 33 cpm of which 3.7 cpm was the expected chance rate and  $3.8 \pm .8$  cpm was the measured chance rate. From this a very rough calculation can be made for the source strength from (32), which gives  $M = 0.07 \text{ mc}$ . At this stage, however, the data are much too rough to give more than an order of magnitude. A more precise measurement

showed the source strength to be 0.13 mc.

Measurements were taken of the various counting rates and approximate calculations were made in order to obtain some idea of the relative contributions to the chance counting rate.

The data used were:

$$\begin{aligned} N_1 &= 20\,000 \text{ cpm} & N_t &= 8.7 \text{ cpm} \\ N_2 &= 100\,000 \text{ cpm} & N_{f1} &= 1.9 \text{ cpm} \\ N_I &= 35\,000 \text{ cpm} & N_{f2} &= 10.7 \text{ cpm} \\ N_{II} &= 120\,000 \text{ cpm} \\ t &= 1 \text{ usec} & t_f &= 25 \text{ nsec.} \end{aligned}$$

Calculation of the terms in (27) gives:

$$\begin{aligned} 2 t(N_{f1}N_2 + N_{f2}N_1) &= 0.007 \text{ cpm} \\ 3 t^2 N_1 N_2 N_f &= 0.00000016 \text{ cpm} \\ 4 t_f t N_1 N_2 (N_I + N_{II}) &= 0.009 \text{ cpm} \\ 6 t^2 t_f N_1 N_2 N_I N_{II} &= 0.00000016 \text{ cpm} \\ 2 t_f N_1 N_2 &= 1.7 \text{ cpm.} \end{aligned}$$

It was apparent that the last term made the only significant contribution, so all other terms were neglected.

#### 4. Determination of Correction for Finite-Size Detectors

A  $\text{Na}^{22}$  source was mounted on the coincidence table and coincidence rates were taken at nine points about  $180^\circ$ . The annihilation radiation consists of coincident 0.5 MeV gamma

rays at an angle of  $180^\circ$ . The chance coincidence rates were subtracted, and the data were plotted. A smooth curve was drawn through the points. The half width at half maximum was measured to be  $b_0 = 6^\circ 15' \pm 5.5'$ . Each detector was then assumed to subtend a cone of solid angle 0.027 steradian.

Note that the energy of the annihilation radiation was not the same as that of either gamma ray from  $\text{Ni}^{60}$ . A better but more complicated procedure for finding the half-angle  $b_0$  experimentally would have been to use a well collimated beam of the same energy as each of the gamma rays.

Solid angle correction factors were calculated from (50).

$$Q_2 Q_2 = 0.9823 \pm .0005.$$

$$Q_4 Q_4 = 0.9420 \pm .0001.$$

The theoretical directional correlation function for the  $\text{Ni}^{60}$  cascade (14) is attenuated to

$$\bar{W}(\theta) = 1 + 0.100 P_2(\cos \theta) + 0.0086 P_4(\cos \theta)$$

### 5. Reduction of Error at $135^\circ$

Since there are no odd Legendre polynomial terms in the directional correlation function, it is symmetric about  $90^\circ$  and  $180^\circ$ . This means that the slope is zero at these two angles thus making them ideal experimentally since a small systematic error in the angles contributes very little error to the measurement. At  $135^\circ$ , the other standard angle, the slope is not necessarily zero. Indeed in the case of  $\text{Ni}^{60}$  this is quite near the point of inflection where the slope

is maximum, so that a small error in the angle setting at  $135^\circ$  may contribute greatly to the error in the measurement.

It was thought that a systematic error at  $135^\circ$  could be eliminated by taking part of the measurements at  $135^\circ$  and part at  $225^\circ$  and adding the counts as if they were all taken at  $135^\circ$ . It was found that the counting rates at these two angles differed by less than the statistical variation after a total of almost 20 000 counts had been taken; nevertheless these measurements were still considered to provide an additional check on the operation of the experimental apparatus.

There are, of course, two other angles that might be used in this method, namely  $45^\circ$  and  $315^\circ$ , but these cannot be realized experimentally at the present time because of the apparatus.

#### 6. Analysis of $\text{Ni}^{60}$ Correlation Data

The  $\text{Co}^{60}$  source was centered on the coincidence table so that the counting rate in the movable detector varied not more than one per cent over the range of angles used. A singles spectrum was observed from each detector. The discriminators on the fast unit were set just above the Compton edge of the 1.17 MeV peak. The single channel analyzers of the slow unit were similarly set. In this way both photopeaks in both channels were used, and the true coincidence rate was effectively doubled.

After the initial setup procedure a series of runs with  $\theta$  equal to  $90^\circ$ ,  $135^\circ$ ,  $180^\circ$ ,  $225^\circ$ , and  $270^\circ$  were taken in which

Table IV. Directional correlation data.

Angle between detectors	Time in min	Counts from fixed detector	Counts from movable detector	True plus chance counts
90°	13.88	269 524	900 003	84
135°	13.69	264 609	900 000	71
180°	13.97	270 537	900 001	82
225°	14.25	288 382	900 000	74
270°	14.08	288 011	900 001	79
225°	14.28	288 597	900 001	72
180°	13.92	281 730	900 000	65
180°	14.05	284 747	900 000	77
135°	13.74	276 491	900 001	74
90°	13.94	278 090	900 004	62
90°	13.90	276 871	900 002	73
135°	13.74	271 586	900 000	81
180°	13.90	275 289	900 001	87
225°	14.18	281 495	900 000	75
270°	13.82	289 448	900 001	63
225°	14.21	295 566	900 001	65
180°	13.92	289 850	900 002	74
135°	13.87	288 235	900 002	68
90°	14.24	288 115	900 002	62
135°	14.25	288 446	900 000	84
180°	14.72	298 830	900 001	90
225°	15.06	306 215	900 001	67
270°	14.71	312 021	900 002	75
225°	14.92	314 948	900 001	79
180°	14.56	308 442	900 001	80
135°	14.28	300 405	900 001	92
90°	14.35	297 049	900 001	83
135°	14.17	290 466	900 002	93
180°	14.54	297 837	900 001	86
225°	14.86	303 828	900 002	89
180°	14.44	296 997	900 002	97
135°	14.17	290 320	900 003	97
90°	14.14	290 789	900 001	84
135°	14.11	289 007	900 003	73
180°	14.42	296 548	900 001	77
225°	14.73	303 352	900 002	85

a total of 67 752 coincidence counts were obtained in 8276.23 minutes of actual counting time. Intermittently between these runs various checks were made. Singles rates were counted for short intervals, waveforms were checked on an oscilloscope, and spectra were taken on a multichannel analyzer.

Table IV shows a portion of the data. In order to reduce the effect of a slightly non-centered source, it is standard practice to normalize the coincidence rates by dividing by the appropriate singles counting rates in the movable counter for each angle. It was thought that if data were taken up to a preset number of counts in the movable detector, this normalization would be unnecessary for a quick check on the data. Note that the scaler had some difficulty in turning off at exactly 900 000 counts. If the counting rate in the movable detector is calculated for a particular angle, it is seen that in general the counting rate decreased with time. These data were all taken within a ten hour period, which is extremely short compared to 5.3 years, the half-life of  $\text{Co}^{60}$ . The change in counting rate was apparently an electronics instability.

Table V.  $\text{Ni}^{60}$  directional correlation data.

angle	time	$0^\circ$ counts	$90^\circ$ counts	true + chance
$90^\circ$ - $270^\circ$	1548.40 min	30 676 393	134 843 117	11 684
$135^\circ$ - $225^\circ$	2562.17 min	50 870 273	217 082 741	19 835
$180^\circ$	2725.66 min	53 931 282	239 154 205	23 231

The wide variation in the number of counts in the fixed detector is expected since the statistical error is composed of two parts. The fixed detector counting rate varies statistically in itself, and the time varies statistically due to taking a preset number of counts in the movable detector which has a statistically varying counting rate.

The analysis went as follows: From the singles rates, the times, and the previous determination of the resolving time, the number of chance counts was calculated for each angle and subtracted from the right hand column of Table V giving the numbers of true coincidence counts for each angle.

The background rate in the movable detector, taken before the source was placed on the apparatus, was 665 cpm. The total number of expected background counts was calculated and subtracted from the number of counts from the movable detector for each angle. The resulting numbers were divided into the respective numbers of true counts to normalize for a slightly off center source.

Errors were propagated according to the standard methods. Three numbers were obtained which were proportional to the normalized true coincidence counting rates:

$$N(90^\circ) = (709 \pm 9) \times 10^{-4} = N_1$$

$$N(135^\circ) = (756 \pm 7) \times 10^{-4} = N_2$$

$$N(180^\circ) = (817 \pm 7) \times 10^{-4} = N_3$$

These numbers are proportional to the directional correlation function. A best constant of proportionality was determined

from a least squares fit to  $\bar{W}(\theta)$  at the three angles.

$$S = \sum (N_i - k \bar{W}(\theta_i))^2$$

$$0 = \frac{dS}{dk} = \sum 2(N_i - k \bar{W}(\theta_i))(-\bar{W}(\theta_i))$$

Then we obtain  $k = 0.0738$ . The experimentally observed values of the directional correlation function at the three angles are:

$$\bar{W}'(90^\circ) = 0.9634 \pm .0117$$

$$\bar{W}'(135^\circ) = 1.0204 \pm .0099$$

$$\bar{W}'(180^\circ) = 1.0988 \pm .0094$$

These numbers were fitted by using White's matrix (38) to yield the experimentally observed directional correlation function for the  $Ni^{60}$  cascade as

$$\begin{aligned} \bar{W}'(\theta) = 1.00 + (0.094 \quad 0.011)P_2(\cos \theta) \\ + (0.0087 \quad 0.010)P_4(\cos \theta). \end{aligned}$$

This is to be compared with the expected correlation function derived in section IV.4,

$$\bar{W}(\theta) = 1 + 0.100 P_2(\cos \theta) + 0.0086 P_4(\cos \theta).$$

Although the errors are rather large, the directional correlation function can provide very useful information. For instance, it can be shown that if the first gamma ray is mixed, the error in  $A_2$  limits the intensity of any  $M3$  component to less than 0.03%.

## V. CONCLUSION

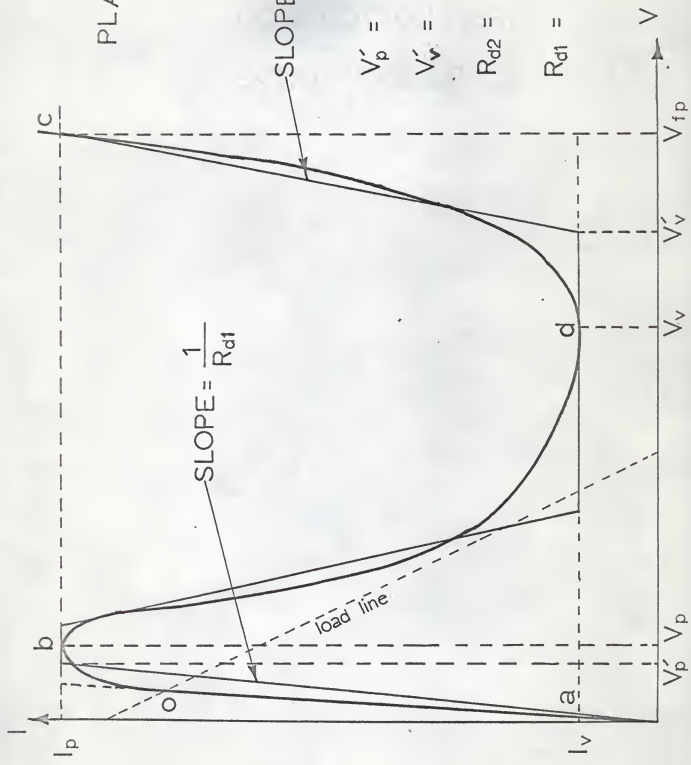
A tunnel diode fast coincidence circuit was constructed and the various properties determined to be as reported in the literature. A commercial circuit of a similar design was used in a directional correlation experiment, and the results were shown to agree with theory. It is concluded that with proper attention to the inherent problems, such as double pulsing, the equipment can be used in this type of experiment.

## VI. ACKNOWLEDGMENTS

The author takes this opportunity to acknowledge and thank Dr. Louis Ellsworth for his guidance and assistance in completing this work. The author also wishes to thank Dr. Charles E. Mandeville and Dr. V. R. Potnis.

## VII. PLATES

PLATE I



SLOPE =  $\frac{1}{R_{d1}}$

SLOPE =  $\frac{1}{R_{d2}}$

$V_p' = 0.75 V_p$

$V_v' = \frac{V_{fp} + V_v}{2}$

$R_{d2} = \frac{V_{fp} - V_v'}{l_p - l_v}$

$R_{d1} = \frac{0.75 V_p}{l_p}$

$V_p'$   $V_p$

$V_v'$   $V_v$

$V_{fp}$

V

I

$l_p$

b

O

a

$l_v$

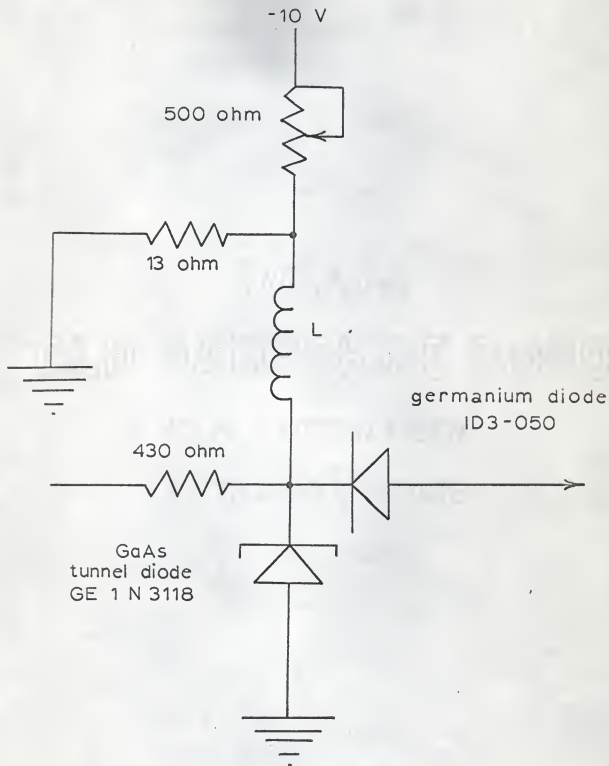
d

load line

EXPLANATION OF PLATE II

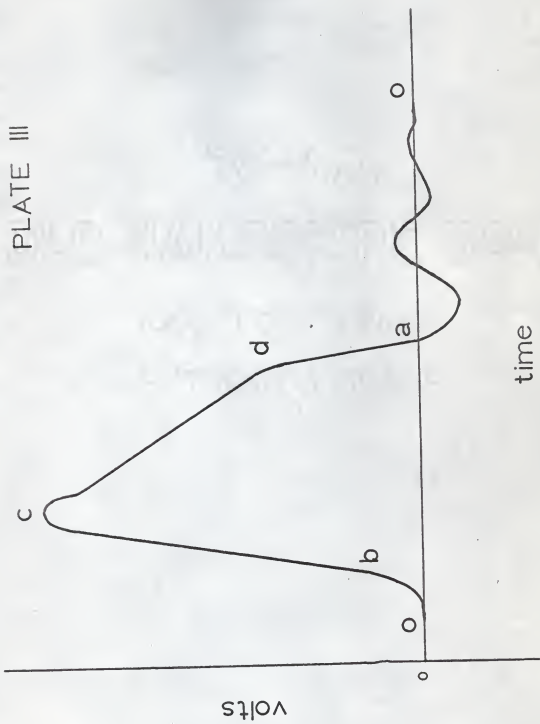
The basic tunnel diode univibrator.

## PLATE II



EXPLANATION OF PLATE III

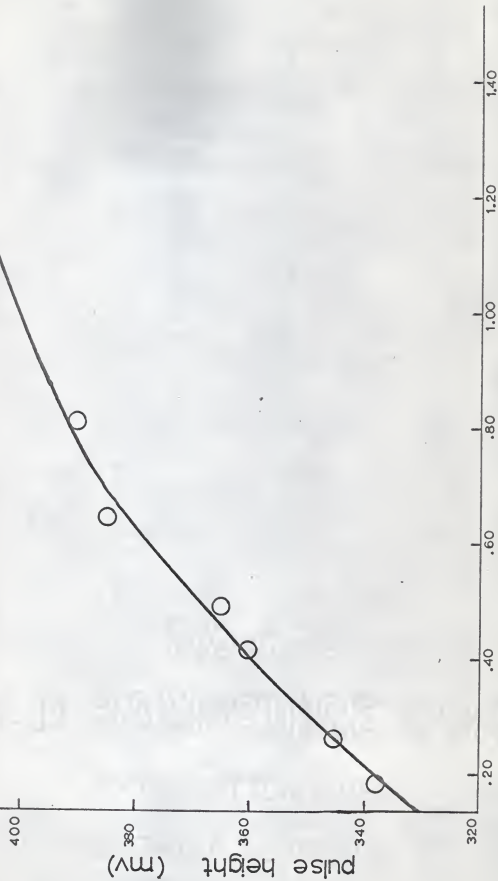
Output pulse of a univibrator.



EXPLANATION OF PLATE IV

A plot of pulse height vs.  
inductance for the univibrator.

PLATE IV



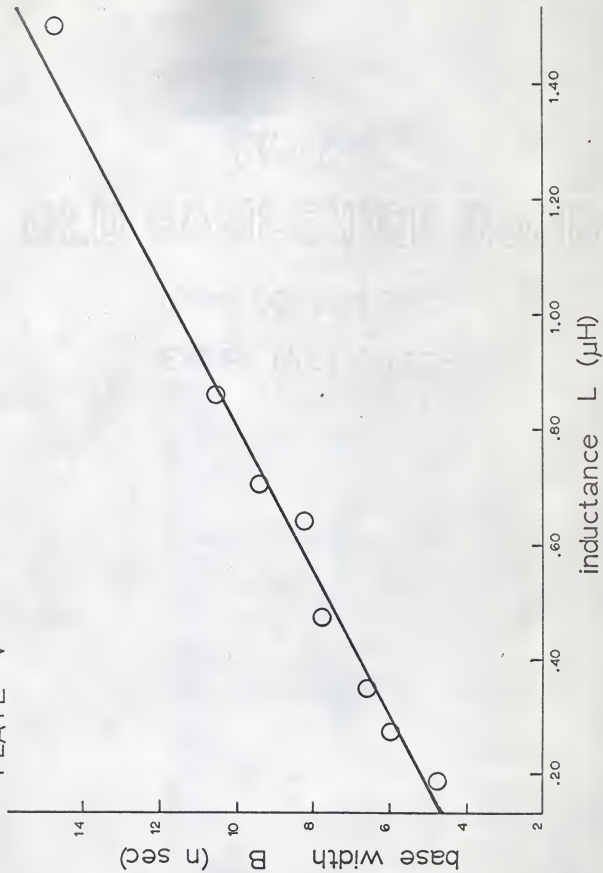
inductance L (μH)

pulse height (mv)

EXPLANATION OF PLATE V

A plot of the base width of the output pulse of a univibrator versus the inductance of the inductor shown in the circuit.

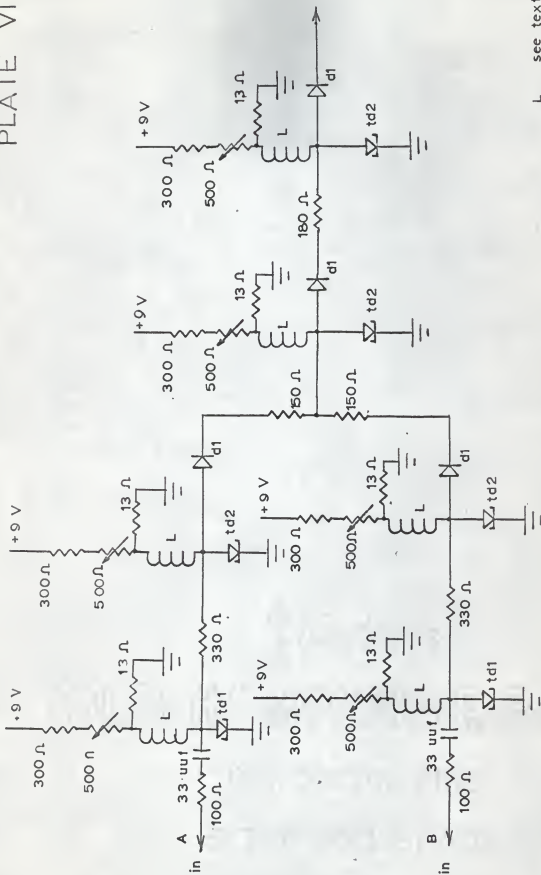
## PLATE V



EXPLANATION OF PLATE VI

The complete coincidence unit  
using six tunnel diode  
univibrators.

PLATE VI



L see text  
d1 ID3-050  
td1 TD 104  
td2 1N311B

tunnel diode coincidence circuit

EXPLANATION OF PLATE VII

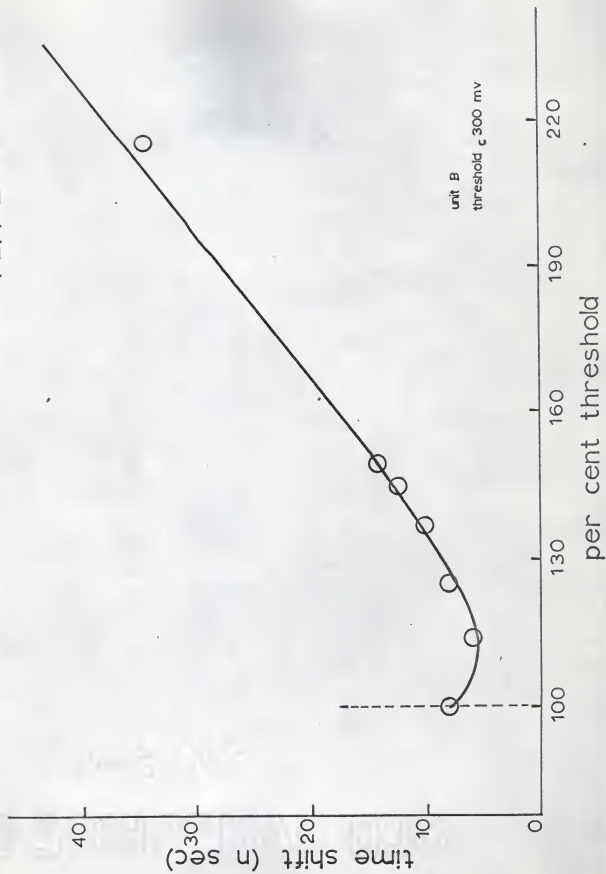
(upper) Nanosecond Systems fast coincidence modules.  
(lower) Fast coincidence unit constructed in the laboratory.



EXPLANATION OF PLATE VIII

A plot showing the slewing  
characteristic of the coincidence  
unit constructed in the laboratory.

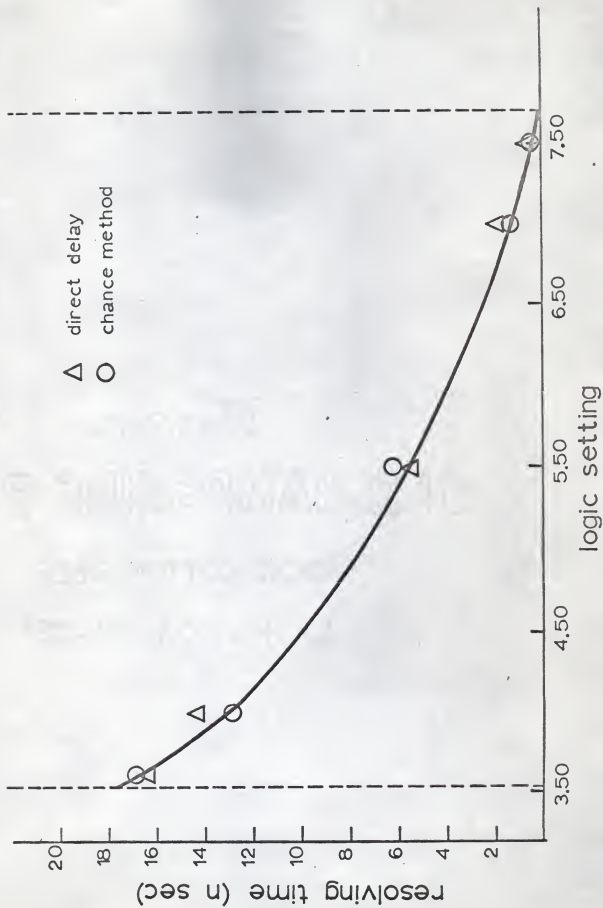
PLATE VIII



#### EXPLANATION OF PLATE IX

A plot of the resolving time of the Nanosecond coincidence unit versus the setting of the logic knob. The inductor used was 1.00  $\mu\text{H}$ . The resolving time was determined by two methods and it is seen that the results of the two are in good agreement.

PLATE IX

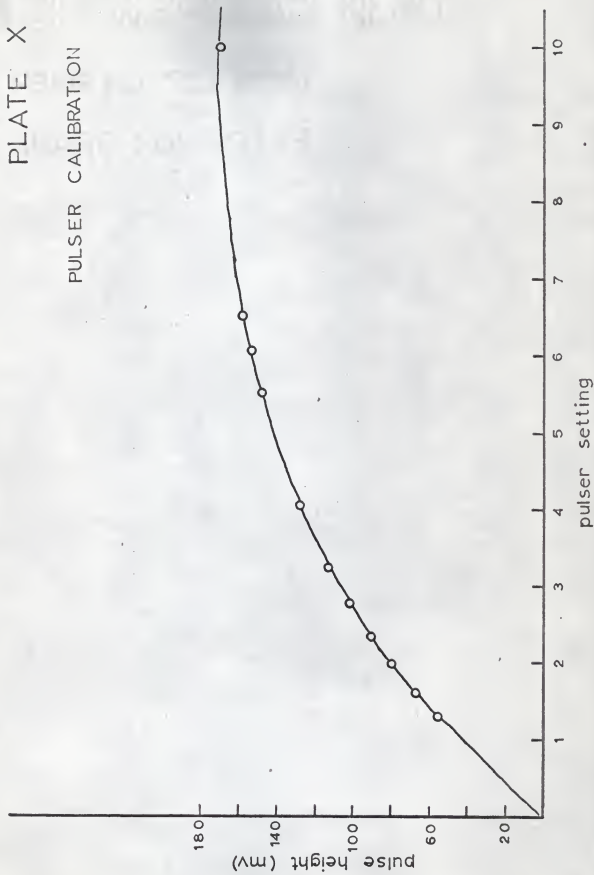


EXPLANATION OF PLATE X

A plot showing the output pulse height of the pulser when fed into a 50 ohm line.

## PLATE X

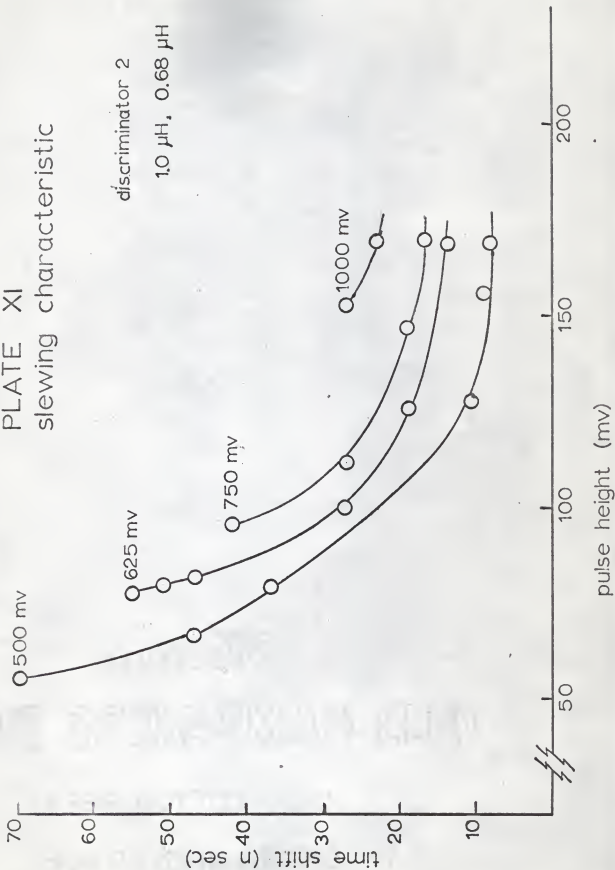
## PULSER CALIBRATION



EXPLANATION OF PLATE XI

A plot showing the slewing characteristic of the Nanosecond equipment including amplifier for various thresholds. The abscissa is the input pulse height before amplification. The curves are labeled with the setting of the discriminator knob.

PLATE XI  
slewing characteristic



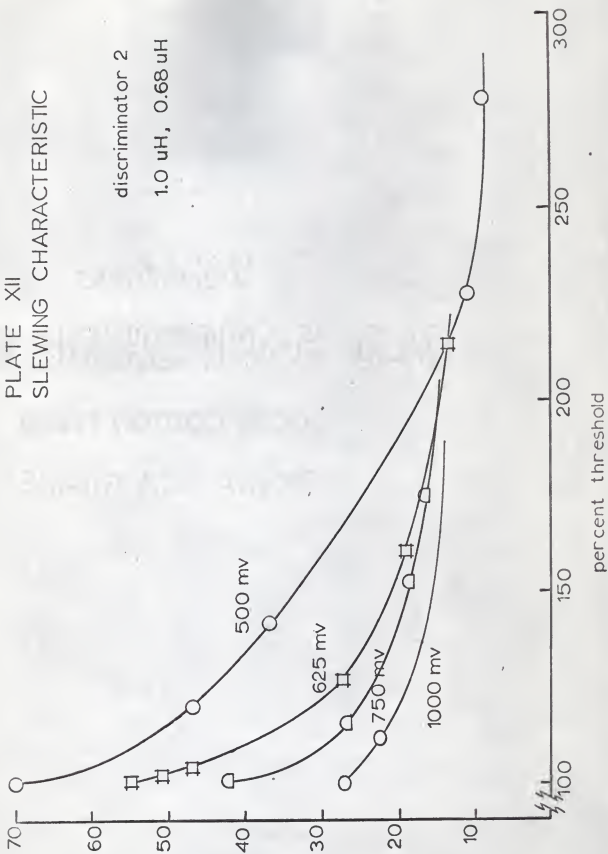
EXPLANATION OF PLATE XII

The same data used in Plate XI  
are replotted with the abscissa  
as per cent of threshold.

PLATE XII  
SLEWING CHARACTERISTIC

discriminator 2

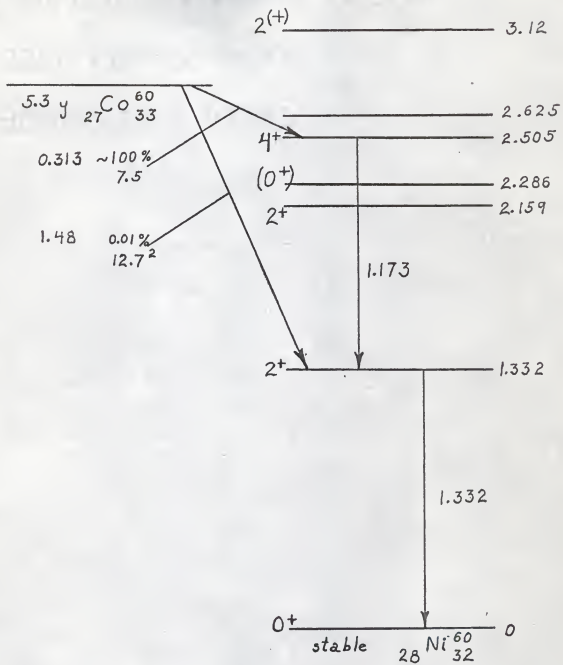
1.0  $\mu$ H, 0.68  $\mu$ H



EXPLANATION OF PLATE XIII

The decay scheme of  $\text{Co}^{60}$  showing the two gamma rays of interest. All energies are in Mev. Although the spins of some states of  $\text{Ni}^{60}$  are still uncertain, the energies, spins, and parities of the states involved in the directional correlation measurement are well established.

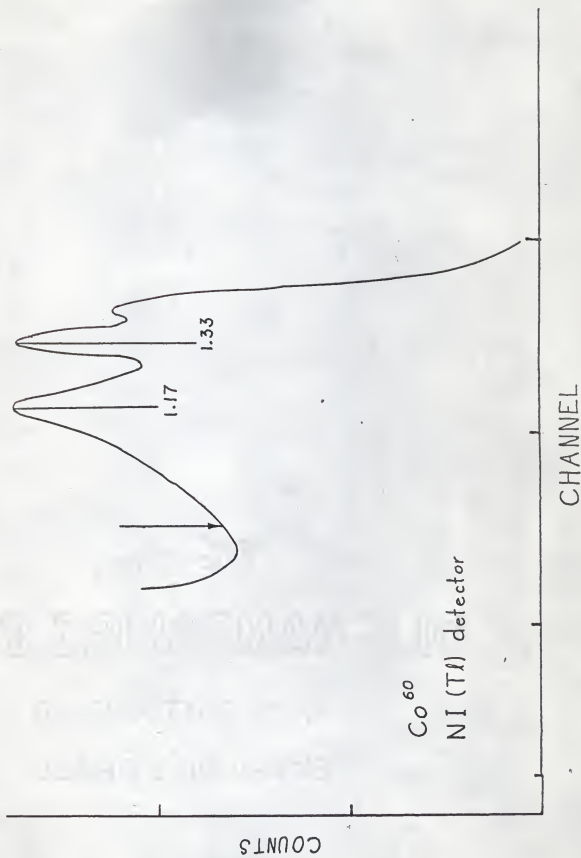
## PLATE XIII



EXPLANATION OF PLATE XIV

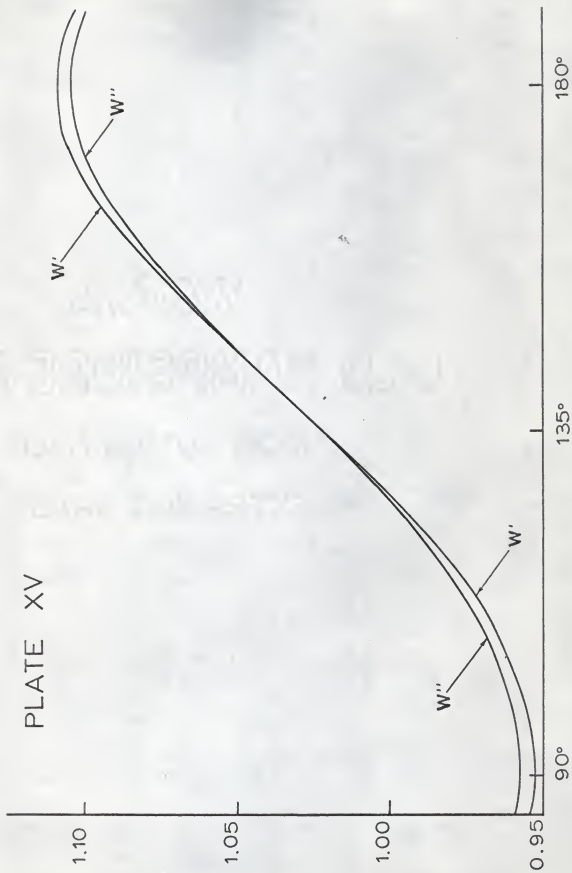
A singles spectrum of  $\text{Co}^{60}$  showing the two photopeaks. The arrow shows the approximate setting of the discriminators. The extra peak to the right is a sum peak due to the high counting rate used.

PLATE XIV



EXPLANATION OF PLATE XV

A plot of the directional  
correlation data.



## VIII. REFERENCES

1. Adler, A., M. Palmai, and V. Perez-Mendez  
100 Mc/s tunnel diode discriminator and pulse shaper. Nuc. Instr. Meth. 13:197. 1961.
2. Artiges, H. C., and J. C. Brun  
Circuits a coincidences rapides utilisant des transistors a avalanche. J. Phys. Rad. 22:53. 1961.
3. Bay, A.  
A new type of high-speed coincidence circuit. Rev. Sci. Instr. 22:397-400. 1951.
4. Bay, A., and G. Papp  
Coincidence device of  $10^{-8}$ - $10^{-9}$  second resolving power. Rev. Sci. Instr. 19:565. 1948.
5. Beller, L. S.  
N-sec scintillation coincidence spectrometer system with high reliability. Rev. Sci. Instr. 34:1001-1006. 1963.
6. Biedenharn, L. C., and M. E. Rosé  
Theory of angular correlation of nuclear radiations. Phys. Rev. 25:729-777. 1953.
7. Bjerke, Arthur A., Quentin A. Kerns, and Thomas A. Nunamaker. Pulse shaping and standardizing of photo-multiplier signals. Nuc. Instr. Meth. 15:249-267. 1962.
8. Bohan, W. A., and A. J. Wager  
The effects of steady state and pulsed nuclear radiation on GaAs tunnel diodes. Ire Trans. on Nuc. Sci. NS-9(1):346-354. 1962.
9. Bonitz, M.  
Modern multi-channel time analyzers in the nano-second range. Nuc. Instr. Meth. 22:238-252. 1963.
10. Bret, George C., and Erwin F. Schrader  
Fast tunnel diode circuits for NaI(Tl) detectors. Nuc. Instr. Meth. 13:177. 1961.
11. Chase, Robert L.  
Multiple coincidence circuit. Rev. Sci. Instr. 31:945-949. 1960.

12. Chase, Robert L.  
Nuclear Pulse Spectrometry. New York: McGraw-Hill,  
1961. 221 p.
13. Dill, H. G.  
New ways to trigger avalanche pulse circuits.  
Proc. IRE 49(6):1093. 1961.
14. Draegert, David A.  
Measurements of two properties of cascade gamma rays,  
Master's Thesis, Kansas State University, 1964.
15. Dunworth, J. V.  
The application of the method of coincidence counting  
in nuclear physics. Rev. Sci. Instr. 11:167-180.  
1940.
16. Elmore, W.  
Coincidence circuit for a scintillation detector of  
radiation. Rev. Sci. Instr. 21:649. 1950.
17. Feingold, A. M., and Sherman Frankel  
Geometrical corrections in angular correlation  
measurements. Phys. Rev. 97:1025-1030. 1955.
18. Frauenfelder, H., and R. M. Steffen in  
Alpha-, beta-, gamma-ray spectroscopy. Amsterdam:  
North-Holland, 1965.
19. Fusca, James A.  
Tunnel diodes may cut transistor costs.  
Aviation Week 71:7. 1959.
20. Garwin, R. L.  
A useful fast coincidence circuit. Rev. Sci. Instr.  
21:569. 1950.
21. Gentile, Sylvester P.  
Basic theory and application of tunnel diodes.  
Princeton: Van Nostrand, 1962. 295 pp.
22. Giorgis, J., and others.  
Tunnel diode manual. Liverpool, New York: General  
Electric, 1961. 97 pp.
23. Gorodetzky, S., and others.  
Circuit de coincidence a diodes tunnel. Nuc. Instr.  
Meth. 14:205-208. 1961.

24. Gorodetzky, S., and others.  
Sur un circuit rapide de mise en forme a seuil  
reglable utilisant des diodes tunnel. Nuc.  
Instr. Meth. 13:282. 1961.
25. Harrison, W., and R. Foote.  
Tunnel diodes increase digital circuit switching  
speeds. Electronics 34(32):154. 1961.
26. Hazoni, Y.  
A fast flip-flop circuit utilizing tunnel diodes.  
Nuc. Instr. Meth. 13:95. 1961.
27. Helmut, Paul  
Higher order chance coincidences in a fast-slow  
coincidence arrangement. Nuc. Instr. Meth. 9:131.  
1960.
28. Howland, B., and others.  
Electronics for Cosmic-Ray Experiments.  
Rev. Sci. Instr. 18:551. 1947.
29. Infante, G., and F. Pandarese  
The tunnel diode as a threshold device; theory and  
application. Nuclear Electronics Vol. III. Vienna:  
International Atomic Energy Agency, 1962.  
pp 29-40.
30. Kallmann, H., and C. A. Accardo  
Coincidence experiments for noise reduction in  
scintillation counting. Rev. Sci. Instr. 21:48.  
1950.
31. Krebs, A. T.  
Early history of the scintillation counter. Science  
122:17. 1955.
32. Lawson, J. S., and H. Frauenfelder  
The correction for finite angular resolution in  
directional correlation measurements. Phys. Rev.  
91:649-652. 1953.
33. Lundby, A.  
Delayed coincidence circuit for scintillation  
counters. Rev. Sci. Instr. 22:324. 1951.
34. Mayer-Kuckuk, T., and R. Nierhaus  
Über die bestimmung der zufälligen koinzidenzen  
in schnell-langsam koinzidenz-anordnungen. Nuc.  
Instr. Meth. 8:76-78. 1960.

35. McGervey, John D.  
A pulse resolver using tunnel diodes. Nuc. Instr. Meth. 14:351-352. 1961.
36. Miller, Barry  
Tunnel diode applications investigated. Aviation Week 71:72. 1959.
37. Rose, M. E.  
The analysis of angular correlation and angular distribution data. Phys. Rev. 91:610-615. 1953.
38. Schram, E., and R. Lombaert  
Organic scintillation detectors. London: Elsevier, 1963.
39. Shera, E. Brooks, K. J. Casper, and B. L. Robinson  
Analysis of chance coincidences in fast-slow coincidence systems. Nuc. Instr. Meth. 24:482-492. 1963.
40. Shera, E. Brooks  
Further comments on accidental coincidences in fast-slow coincidence systems. Nuc. Instr. Meth. 12:198. 1961.
41. Smaller, B., and E. Avery  
The use of gated-beam tubes in coincidence circuits. Rev. Sci. Instr. 22:341. 1951.
42. Sprokel, G. J.  
A liquid scintillation counter using anticoincidence shielding. IBM Jour. Res. Dev. 7(2):135-145. 1963.
43. Strauss, M. G.  
Timing slow pulses for fast coincidence measurements. Rev. Sci. Instr. 34:1248. 1963.
44. Tarnay, K.  
The maximum power output of the tunnel diode oscillator. Proc. IRE 50(10):2120-2121. 1962.
45. Van Zurk, R.  
Circuit discriminateur d'amplitude utilisant diodes tunnel. Nuc. Instr. Meth. 16:157-162. 1962.
46. Ward, C. B., and C. M. York  
A nanosecond pulse height discriminator. Nuc. Instr. Meth. 23:213-217. 1963.

47. Whetstone, Albert L.  
Improving the tunnel diode univibrator. Rev. Sci.  
Instr. 34:412-413. 1963.
48. Whetstone, A., and S. Kounosu  
Nanosecond coincidence circuit using tunnel diodes.  
Rev. Sci. Instr. 33:423-428. 1962.
49. Yonda, A. H., R. Sugarman, and W. A. Higinbotham  
100 Mc counting system. Nuclear Electronics Vol. III.  
Vienna: International Atomic Energy Agency, 1962.  
pp. 3-13.

A MEASUREMENT OF THE Ni<sup>60</sup> DIRECTIONAL CORRELATION  
WITH A TUNNEL DIODE COINCIDENCE CIRCUIT

by

GARY EDWIN CLARK

B. A., Park College, 1961

---

AN ABSTRACT OF A MASTER'S THESIS

submitted in partial fulfillment of the  
requirements for the degree

MASTER OF SCIENCE

Department of Physics

KANSAS STATE UNIVERSITY  
Manhattan, Kansas

1966

A coincidence circuit with a resolving time of a few nanoseconds has been built using tunnel diodes. The theory of operation is discussed.

The circuit consists of a series of tunnel diode univibrators. Germanium tunnel diodes are used at the inputs to give greater sensitivity and to reduce the time jitter. The first stage of each input is followed by a gallium arsenide tunnel diode univibrator. The purpose of this second stage is to provide a standard pulse of typically 5 nsec width and 100 mV height which is independent of the input pulse height.

The standardized pulses are then fed to a coincidence univibrator through a germanium fast diode which serves to make the circuit unilateral. Standardized pulses from two separate circuits are added linearly in the coincidence unit. The coincidence tunnel diode univibrator is set to fire when the standardized pulses add to give a sum pulse of a certain height, which must be between one and two times the height of a single standard pulse. The coincidence unit is followed by another univibrator which produces a much wider pulse. The output can then be counted by a scaler or used to gate a multichannel analyzer.

A fast germanium diode is used to make the circuit unidirectional. With germanium tunnel diodes in the circuit the voltage changes would be too small to effectively forward bias the fast diode, and the coupling would be primarily through the capacitance of the fast diode, which is bidirectional.

For this reason gallium arsenide tunnel diodes, which have a higher voltage change, are used.

The directional correlation function of the well known  $\text{Ni}^{60}$  transitions was determined experimentally using the tunnel diode circuit. Corrections for detectors of finite size were made. The results agreed well with theory.

Various experimental checks were made of coincidence rates, resolving times, and waveforms. All experimental results were found to agree well with theoretical predictions.